Hindawi
Mathematical Problems in Engineering
Volume 2022, Article ID 2201996, 12 pages
https://doi.org/10.1155/2022/2201996

Research Article

Normality Test for Influence Function of Mining Surface Subsidence Based on Network Observation Station

Pengyu Li,[1] Zhenqi Hu ,[1,2] Yaokun Fu,[1] Gensheng Li,[3] Jiaxin Guo,[1] and Dongzhu Yuan[1]

[1]*Institute of Land Reclamation and Ecological Restoration, China University of Mining and Technology (Beijing), Beijing 100083, China*
[2]*School of Environment Science and Spatial Informatics, China University of Mining and Technology, Xuzhou 221116, China*
[3]*School of Public Policy and Management, China University of Mining and Technology, Xuzhou 221116, China*

Correspondence should be addressed to Zhenqi Hu; huzq@cumtb.edu.cn

Received 5 June 2022; Revised 3 August 2022; Accepted 9 August 2022; Published 5 September 2022

Academic Editor: Punit Gupta

Coal is the primary energy source in China, while underground mining is the mainstream way of coal mining. By triggering surface movement and deformation, underground mining can cause damage to arable land, buildings, roads, and so on, which is detrimental to the ecological environment in the mining area. In order to assess the severity of damage caused by this to the ground buildings and ecological environment in the mining area, it is necessary to predict mining-induced surface subsidence before the mining activities are carried out. Currently, the most used prediction method is the Probability Integral Method. It is based on probabilistic theory to mathematically demonstrate that the surface downwelling caused by underground extraction conforms to normal distribution. However, there is a lack of validation with measured subsidence basin data. Since the 1960s, China has been paying increased attention to the study of mining subsidence. However, there are still few network stations built across China to monitor subsidence basin. Herein, SPSS software is applied to re-analyze these valuable historical data. By analyzing the observation results and comparing them with the calculation results as obtained by using the probability integral method, it can be found out that the surface subsidence in the center of the subsidence basin conforms to normal distribution, not the subsidence at the edge of the subsidence basin. Therefore, it is inevitable for errors to occur at the edge of the subsidence basin when the normal distribution function is used as the mining influence function to calculate the surface subsidence. This conclusion is expected to provide practical reference for the prediction of surface subsidence in coal mines, and this experience can be extended to the mining of other solid minerals.

1. Introduction

Although China has been putting much efforts into the development and utilization of renewable energy [1, 2], coal remains the dominant source of energy [3]. In 2020, the national raw coal production in China amounted to 3.9 billion tons, accounting for 47.3% of the world's total, to which underground mining contributed as high as 85%. Nowadays, China has the highest proportion of coal production and underground mining in the world [4–6]. In order to evaluate the severity of damage caused by mining to ground buildings and ecological environment in the mining area, it is necessary to assess the risk of surface movement and deformation before mining gets underway. So far, the research on surface subsidence in coal mines has been conducted for more than 100 years [7]. There are a wide variety of empirical function models proposed in plenty of studies for specific geological and mining conditions based on the data collected by linear observation stations, such as negative exponential function, hyperbolic function, trigonometric function, etc. [8–11]. In the 1950s, Knothe proposed a mining influence function that conformed to normal distribution according to the observation data [12, 13] by treating the surface movement process caused by mining as a random process, Litwiniszyn put forward the random medium theory, arguing that the mining influence function followed normal distribution as well [14]; In 1965, Liu Baochen and Liao Guohua adopted the probability theory to

mathematically demonstrate that the mining influence function conformed to normal distribution, which led to the Probability Integral Method [15–22]. Among the three calculation methods as mentioned above, the Knothe influence function method assumes that the mining influence function conforms to normal distribution based on the observation data. Differently, Litwiniszyn and Liu Baochen reached their conclusion through the simplified mathematical processing in an ideal state. Despite being based on different assumptions, these three calculation methods lead to the same conclusion, which making people default that the mining influence function obeys the normal distribution. However, there is still a lack of requisite test data.

As the Chinese government attaches increasing significance to addressing the environmental damage caused by surface subsidence [23, 24], it is essential for coal mine productions to comply with national laws and regulations. On the one hand, it is necessary to reduce the surface subsidence caused by mining. On the other hand, it is necessary to take remedial actions in those areas where surface subsidence have occurred. At the same time, in order to reduce the cost of damage compensation incurred by mining for buildings, it is necessary to accurately calculate and evaluate the surface subsidence occurring coal mines. To achieve this purpose, it is essential to evaluate the mining impact function, and to verify the rationality of using the normal distribution as the mining influence function.

To establish whether the subsidence occurring outside the main section of the settlement basin conforms to normal distribution, it is necessary to obtain the measured data for the entire network of observation stations in the basin. In China, surface movement observation did not start until the early 1960s. Up to now, there have been many linear surface movement observation stations built in the mining areas. However, there are still as few as two networks of observation stations built for the Pingdingshan and Chaili coal mines [25]. In this paper, the historical data collected by Chaili coal mine network observation station are reanalyzed in an advanced way to explore the distribution law of mining influence function. According to the research results, a significant calculation error will arise from the practice of taking the normal distribution as the mining influence function at the edge of the subsidence basin. This result will influence the judgment on mining subsidence basin boundary, which affects production safety, land damage, and building damage compensation. The results of this study provide a practical reference for the prediction of surface subsidence in coal mining areas, which can be extended to the mining of other solid minerals.

2. Study Area

The study area is located in Xigang Town, Tengzhou City, which is about 22 km away from the city center of Tengzhou, and its location is shown in Figure 1. In terms of climate, the study area shows the characteristics of temperate arid to monsoon continental climate, with an annual average temperature of 13.6°C. The annual precipitation reaches about 793.0 mm, and the average annual evaporation stands at 1791.7 mm [26, 27]. Geographically, the study area features a lakeside alluvial plain with flat terrain, highly developed road network and dense population. The terrain declines slowly from the northeast to the southwest. Ground elevation decreases from +43.73 m to +35.30 m, with a slope of about 1‰. The soil texture in the area is dominated by clay loam and loam, the sandy clay ratio is moderate, the permeability is high, the soil quality is excellent, the level of soil fertility is satisfactory, and the production capacity is high.

2.1. General Situation of Working Face. The strike length of working face 331 is 540 m, and the inclined length is 136 m. Strike longwall comprehensive mechanized coal mining is adopted for the working face, and the full caving method is applied for roof management. On average, the ground elevation is about +40.0 m, and the mining depth is 132 m. The first-time mining was conducted in July, 1973, and the last-time mining took place in October, 1976. According to the histogram analysis of a borehole near the working face, the overlying strata is 132 m deep on average. The quaternary system results from the interactive deposition of the clay layer and sandstone layer, with a thickness of 71 m. Besides, the sandstone layer is 30 m and the mudstone layer is 31 m in thickness. The overlying strata show a medium hardness in the comprehensive lithology. The coal seam is simple in structure and stability in occurrence, with an average thickness of 1.8 m and an average dip angle of 4°. The false roof is 2–7 m mudstone, and the coal seam floor is grayish black sandy mudstone, 9–14 m. Figure 2 shows the comprehensive histogram of the overlying strata.

2.2. Layout of Observation Stations. In general, there are two types of surface movement observation stations: linear observation station and network observation station [25]. At present, linear observation stations are most commonly seen in China. Usually, the observation line of linear observation station is comprised of strike line and inclination line, which are perpendicular to each other. In some cases, it is possible to set only one or half observation line. For example, the strike length of the working face is too large, the workload of setting the full strike observation line is high, and the observation time is long. In this case, a common practice is to set half of the strike observation line. In another example, one side of the dip direction is affected by the mining of the adjacent working face, which means only half of the dip observation line can be set. The observation line setting scheme depends on the exact purpose of observation and on-site conditions in the setting area. Its selection is based on the practicalities and principle of obtaining as much reliable data as possible. The layout of several different linear observation stations is shown in Figure 3(a).

In the network observation station, the observation points are arranged into a network, so as to monitor the whole area, half area or quarter area of surface movement and deformation, as shown in Figure 3(b). The layout of surface movement network observation stations is treated as the control network for monitoring the whole subsidence

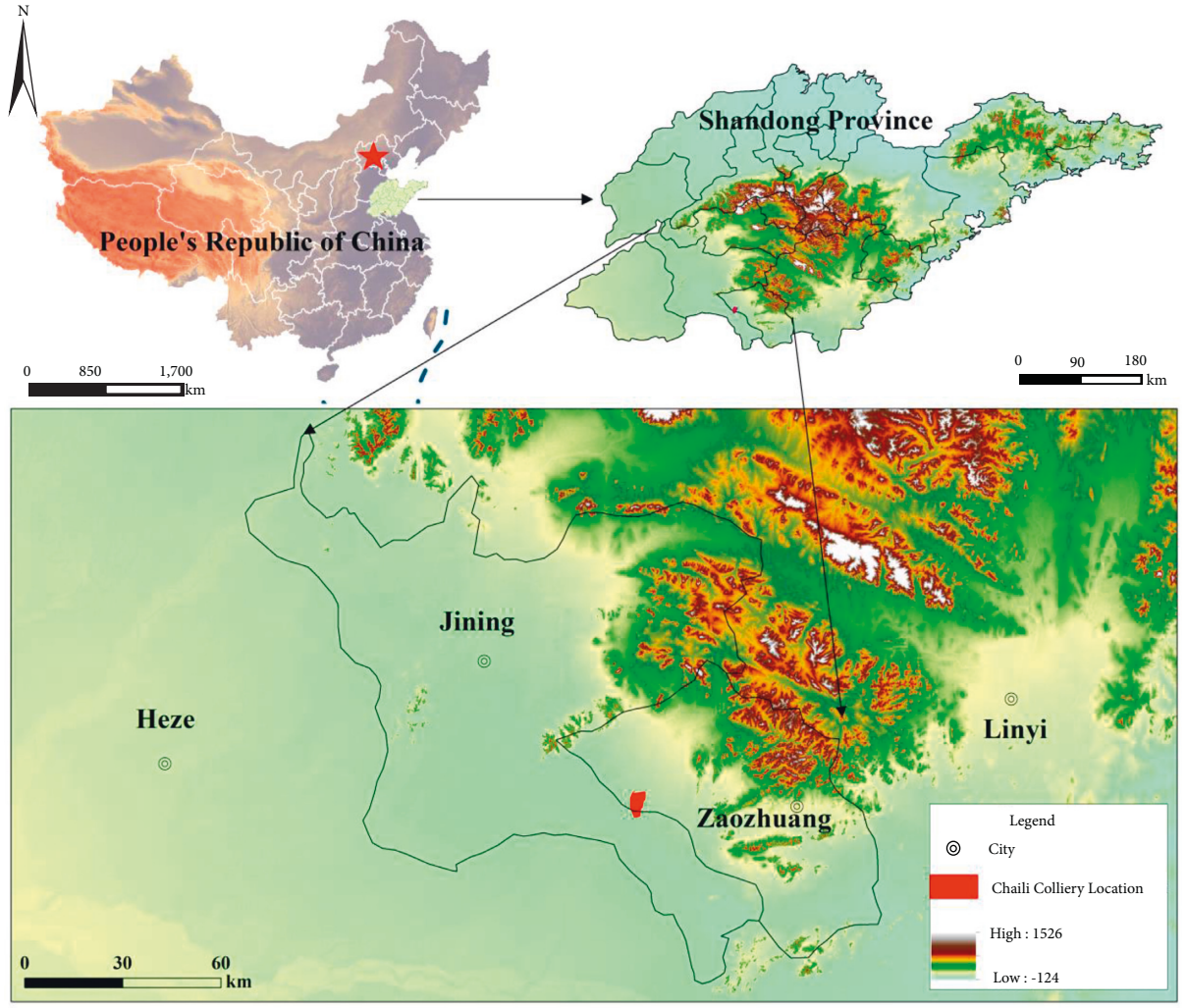

Figure 1: Location of the Chaili colliery.

basin to fully show the movement and deformation law of the whole surface movement basin.

The network observation station involved in this study was established on June 15,1973. After 4 years of observation, the final data of surface subsidence observation were collected. Figure 4 shows the layout of observation station network and embedding of point markers. There are 146 points in total, the distance between two observation stations is 15 m, and there are 20 observation lines, of which 7 are in the strike direction and 13 are in the inclination direction.

After all the points of the observation station are marked, dig pits and bury point markers, which are made of concrete. The top surface of the point mark is sized 250*250 mm, the height is 1000 mm, the mark center is 520 mm iron bar, and the top is engraved with a cross. Theodolite is used to indicate the direction of the observation line at the time of burying stake, and a steel ruler is used to mark the position on the observation line. After all points are buried, the point number is red painted on the top surface of the stake.

The altitude is measured at the observation stations by using precision leveling instruments and a total of 18 leveling measurements. Also, data processing is carried out through the subsidence calculation formula. The formula used to calculate subsidence for point n during the mth time observation is expressed as

$$W_n = H_{n0} - H_{nm}, \tag{1}$$

where W_n represents the subsidence value of point n. H_{n0}, H_{nm} refer to the altitudes at the first and the m-th observation, respectively.

The final subsidence values at each point for the net observation lines are listed in Table 1.

3. Results

3.1. Test Results of the Normal Subsidence of the Observation Line. The commonly used normal test methods can be divided into three categories in general [28]. The first one is graphical representation, which is examined mainly using probability plots (P–P plots) and quantile plots (Q-Q plots). The second one is the kurtosis–skewness joint test. Kurtosis indicates how flattened or steep the top of the frequency

Lithology	Layer Thickness (m)	Layer Depth (m)	Columnar
Clay	5.20	5.20	
Fine-grained sandstone	1.60	6.80	
Clay	2.40	9.20	
Siltstone	1.00	10.20	
Clay	4.80	15.00	
Sandy mudstone	1.40	16.40	
Clay	5.50	21.90	
Medium grained sandstone	1.40	23.30	
Clay	1.60	24.90	
Fine-grained sandstone	0.90	25.80	
Clay	2.80	28.60	
Core-grained sandstone	5.40	34.00	
Clay	1.60	35.60	
Sandy mudstone	2.60	38.20	
Clay	3.20	41.40	
Fine-grained sandstone	4.10	45.50	
Clay	6.90	52.40	
Core-grained sandstone	2.00	54.40	
Clay	4.20	58.60	
Sandy mudstone	0.80	59.40	
Clay	8.50	67.90	
Gravel	3.10	71.00	
Sand shale	31.00	102.00	
Siltstone	30.00	132.00	
Coal	1.80		
Siltstone	0.40		
Core-grained sandstone	14.20		

Figure 2: Comprehensive histogram of overburden of 331 working face.

distribution curve is for the test sample, and skewness is used to indicate the degree to which a distribution deviates from symmetry. The last one is the Kolmogorov Smirnov test (K–S normality test). The latter two are more reliable than graphical representation. Therefore, the kurtosis–skewness joint test and K–S normality test are adopted in this study to verify the normality of surface subsidence with the assistance of SPSS software.

3.1.1. Kurtosis–Skewness Normality Test. The kurtosis and skewness coefficient values of the data are used to determine whether the samples conform to normal distribution or not. If the absolute values of kurtosis coefficient Z_K and skewness coefficient Z_S fall below 1.96 simultaneously, the distribution of sample data is considered to conform to normal distribution. If either or both the absolute values of Z_K or Z_S exceed 1.96, the sample data are considered not to conform to normal distribution [29]. The formulas used to calculate Z_K and Z_S are expressed as follows:

$$Z_K = \frac{K-0}{S_K}, Z_S = \frac{S-0}{S_S}. \tag{2}$$

Where S_K and S_S represent standard error for kurtosis coefficient and skewness coefficient, respectively.

Table 2 depicts the calculation results obtained from the normality test on the subsidence kurtosis and the skewness of the observation lines in the inclination direction. It is found out that the absolute kurtosis coefficient and skewness coefficient values are less than 1.96 during 12 observation lines, the sedimentation profiles of which conform to normal distribution. However, the absolute values of kurtosis coefficient and skewness coefficient of the A13-G13 observation line exceed 1.96, which means the subsidence of this observation line does not follow normal distribution.

Table 3 presents the calculation results obtained from the normality test on the subsidence kurtosis and the skewness of the strike parallel observation lines. The absolute values of the kurtosis coefficient and the skewness coefficient of the seven strike parallel observation lines fall below 1.96, which suggests that the subsidence distribution of the strike parallel observation lines conforms to normal distribution.

3.1.2. K–S Normal Test. The rationale of the K–S normality test is described as follows. To calculate the theoretical cumulative probability value $F(x)$ of the sample data, it is assumed that normal distribution is followed. Then, the actual cumulative probability value $S(x)$ of the sample is calculated. The D-value $D(x)$ between them is calculated as follows:

$$D = \max\left(\left|S(x_i) - F(x_i)\right|\right). \tag{3}$$

D must be corrected into

$$D = \max\left(\max\left(\left|S(x_i) - F(x_i)\right|\right), \max\left(\left|S(x_{i-1}) - F(x_{i-1})\right|\right). \tag{4}$$

SPSS software is directly applicable to calculate the probability value(p-value). As for whether the sample value conforms to the normal distribution, it is determined by whether the significance level is exceeded (0.05 in general) [30]. If the probability value falls below 0.05, it is considered that the test sample does not conform to normal distribution. If the value reaches above 0.05, the test sample is considered to conform to normal distribution.

Table 4 lists the results of normality test conducted on the inclination parallel observation lines. It can be seen clearly from the table that there are 12 observation lines

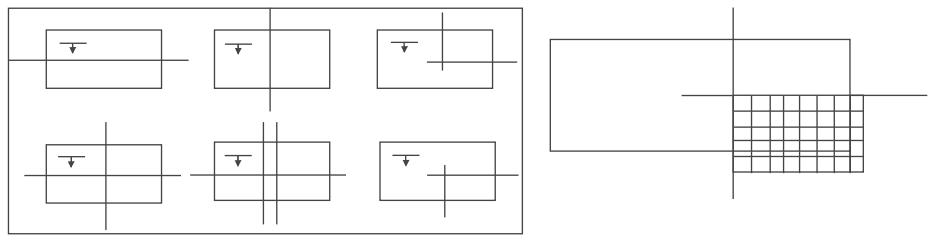

Figure 3: Diagrammatic sketch of linear and network observation stations. (a) are linear observation stations, Observation lines are the main section observation line; (b) is a network observation station.

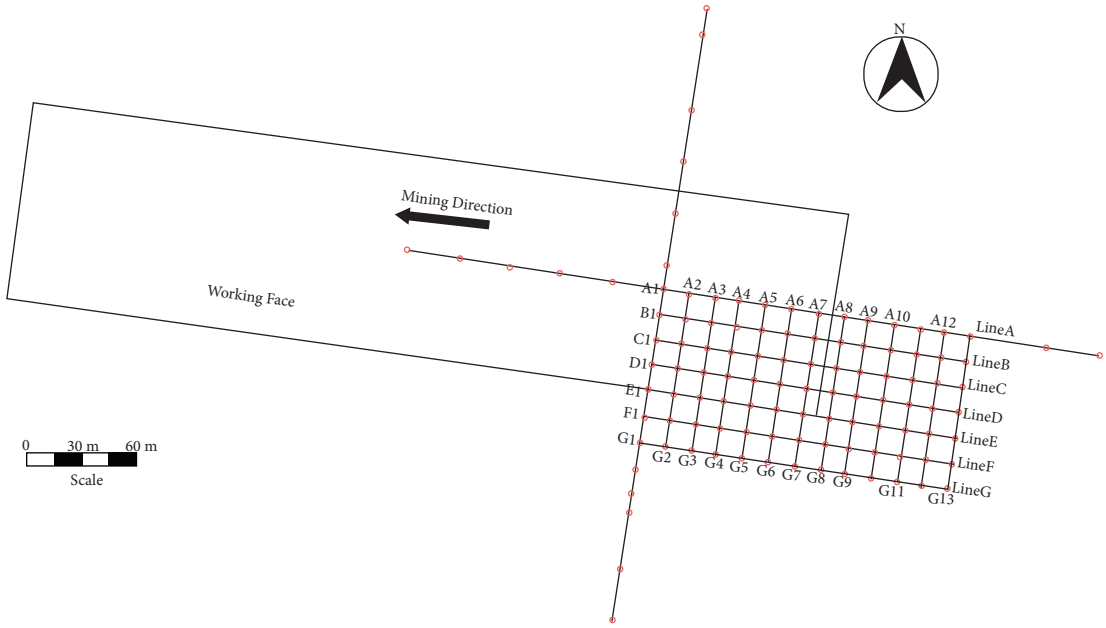

Figure 4: Layout of the network of observation stations.

Table 1: Final subsidence value of network observation station.

Subsidence value/mm	Line A	Line B	Line C	Line D	Line E	Line F	Line G
Line A1–G1	−1318.00	−1263.00	−1087.00	−713.00	−366.00	−162.00	−78.00
Line A2–G2	−1265.28	−1326.15	−1065.26	−698.74	−355.02	−160.38	−70.98
Line A3–G3	−1225.74	−1212.48	−1054.39	−698.74	−338.34	−184.68	−68.64
Line A4–G4	−1212.56	−1199.85	−1054.39	−698.74	−344.04	−163.62	−62.40
Line A5–G5	−1146.66	−1136.7	−967.43	−641.70	−286.47	−118.26	−53.04
Line A6–G6	−948.96	−896.73	−739.16	−456.32	−208.62	−86.33	−45.24
Line A7–G7	−553.56	−505.20	−391.32	−235.29	−139.08	−58.32	−22.62
Line A8–G8	−276.78	−239.97	−195.66	−114.08	−62.22	−43.74	−16.27
Line A9–G9	−92.26	−88.41	−76.09	−49.91	−36.60	−30.78	−14.04
Line A10–G10	−52.72	−50.52	−40.33	−28.52	−22.37	−19.44	−13.66
Line A11–G11	−26.36	−23.73	−21.74	−18.23	−14.64	−13.28	−10.14
Line A12-G12	−13.18	−12.63	−10.22	−14.26	−12.43	−11.34	−8.37
Line A13–G13	−11.23	−9.88	−21.74	−12.67	−10.47	−9.76	−10.14

with a greater p-value than 0.05. That is to say, the subsidence of 12 inclination direction observation lines conforms to normal distribution. Only the p-value of the Line A13-G13 is less than 0.05, which suggests that the subsidence of this observation line does not follow normal distribution.

Table 5 shows the results of normality test on the strike parallel observation lines. Since the p-value of the strike parallel observation lines are significantly higher than 0.05, it is judged that the subsidence distribution of each observation line parallel to the strike of the main section conforms to normal distribution.

Table 2: Results of the kurtosis–skewness normality test of the observation lines in the inclination direction.

Observation lines	N	Normal parameter		K	S_K	Z_K	S	S_S	S_K
		Mean value	Standard deviation						
LineA1–G1	7	−712.429	522.116	0.036	0.794	0.045	−2.171	1.587	1.368
LineA2–G2	7	−705.973	524.506	0.003	0.794	0.005	−2.139	1.587	1.348
Line A3–G3	7	−683.287	492.890	0.075	0.794	0.094	−2.216	1.587	−1.396
Line A4–G4	7	−676.514	492.484	0.101	0.794	0.127	−2.214	1.587	−1.395
Line A5–G5	7	−621.466	474.331	0.056	0.794	0.071	−2.247	1.587	−1.416
Line A6–G6	7	−479.050	387.682	−0.073	0.794	−0.092	−2.180	1.587	−1.374
Line A7–G7	7	−272.199	213.994	−0.211	0.794	−0.266	−1.905	1.587	−1.200
Line A8–G8	7	−135.531	102.435	−0.282	0.794	−0.355	−1.872	1.587	−1.180
Line A9–G9	7	−53.821	32.265	−0.003	0.794	−0.004	−2.020	1.587	−1.273
Line A10–G10	7	−32.509	15.486	−0.286	0.794	−0.360	−1.813	1.587	−1.142
Line A11–G11	7	−18.303	5.937	−0.004	0.794	−0.005	−1.464	1.587	−0.922
Line A12–G12	7	−11.776	1.980	0.732	0.794	0.922	0.166	1.587	0.105
Line A13–G13	7	−12.270	4.296	−2.365	0.794	−2.979	5.767	1.587	3.634

Table 3: Results of the kurtosis–skewness normality test of the observation lines in the strike direction.

Observation lines	N	Normal parameter		K	S_K	Z_K	S	S_S	S_K
		Mean value	Standard deviation						
Line I	13	−626.407	564.244	−0.065	0.616	−0.106	−2.097	1.191	−1.761
Line A	13	−612.712	562.983	−0.115	0.616	−0.187	−2.081	1.191	−1.748
Line B	13	−517.287	478.136	−0.142	0.616	−0.231	−2.100	1.191	−1.7638
Line C	13	−336.938	314.855	−0.190	0.616	−0.308	−2.091	1.191	−1.7568
Line D	13	−168.946	150.802	−0.224	0.616	−0.364	−1.965	1.191	−1.6508
Line E	13	−81.687	67.439	−0.390	0.616	−0.634	−1.684	1.191	−1.414
Line F	13	−36.426	27.040	−0.384	0.616	−0.623	−1.781	1.191	−1.495

Table 4: Results of the K–S normality test of each line in the inclination direction.

Observation lines	N	Normal parameter		Statistic	p
		Mean	Standard deviation		
Line A1–G1	7	−712.429	522.116	0.508	0.959
Line A2–G2	7	−705.973	524.506	0.481	0.975
Line A3–G3	7	−683.287	492.890	0.537	0.936
Line A4–G4	7	−676.514	492.484	0.548	0.925
Line A5–G5	7	−621.466	474.331	0.518	0.951
Line A6–G6	7	−479.050	387.682	0.492	0.969
Line A7–G7	7	−272.199	213.994	0.428	0.993
Line A8–G8	7	−135.531	102.435	0.507	0.960
Line A9–G9	7	−53.821	32.265	0.486	0.972
Line A10–G10	7	−32.509	15.486	0.458	0.985
Line A11–G11	7	−18.303	5.937	0.423	0.994
Line A12–G12	7	−11.776	1.980	0.532	0.940
Line A13–G13	7	−12.270	4.296	0.847	0.047

There is consistence shown in the conclusions between the normal test of the kurtosis–skewness and the K–S normal test. Among the 20 observation lines tested, only observation line A13–G13, which is the farthest away from the subsidence basin center, does not conform to normal distribution. However, the subsidence of the other strike and inclination parallel observation lines conforms to normal distribution, i.e., the subsidence in the surface of the mining area conforms to normal distribution overall.

3.2. Calculation Error of the Surface Subsidence at Any Point. Based on the Knothe influence function method [13], Figure 5 is built to show the working face and the calculation coordinate system of the horizontal coal seam, where l represents the calculation length of the trend; L indicates the calculation width of the tendency; and $A(x, y)$ denotes any point on the surface.

Since the probable directions of x and y are independent of each other, the subsidence at $A(x, y)$ is expressed as follows:

$$\begin{aligned} W(x,y)_A &= W_{\max}\iint_F f(x,y)dF \\ &= W_{\max}\iint_F f(x)f(y)dxdy, \\ f(x) &= \frac{1}{r}e^{-\pi\frac{x^2}{r^2}}, \\ f(y) &= \frac{1}{r}e^{-\pi\frac{y^2}{r^2}}, \end{aligned} \tag{5}$$

where $W_{\max}$ represents the maximum surface subsidence; r indicates the main mining influence radius; $f(x)$, $f(y)$ denotes the Knothe influence function, which follows a $N(0, \sigma^2)$ distribution, and $\sigma = r/\sqrt{2\pi}$.

O represents the coordinate origin in Figure 5, so that the subsidence at $A(x, y)$ is expressed as follows:

Table 5: Results of the K–S normality tests of each observation line in the strike direction.

Observation lines	N	Normal parameter		Statistic	p
		Mean value	Standard deviation		
Line I	13	−626.407	564.244	0.767	0.599
Line A	13	−612.712	562.983	0.753	0.623
Line B	13	−517.287	478.136	0.762	0.607
Line C	13	−336.938	314.855	0.800	0.543
Line D	13	−168.946	150.802	0.800	0.544
Line E	13	−81.687	67.439	0.671	0.759
Line F	13	−36.426	27.040	0.842	0.477

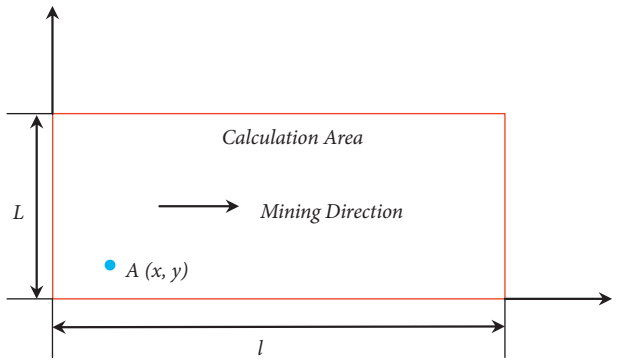

Figure 5: Calculation coordinate system.

$$
\begin{aligned}
W(x,y)_A &= \frac{W_{\max}}{r^2}\int_{-x}^{l-x} e^{-\pi\left(\frac{x}{r}\right)^2}dx\int_{-y}^{l-y} e^{-\pi\left(\frac{y}{r}\right)^2}dy \\
&= W_{\max}\times\frac{1}{2}\left\{\left[erf\left(\sqrt{\pi}\,\frac{x}{r}\right)+1\right]\right. \\
&\quad \left.-\left[erf\left(\sqrt{\pi}\,\frac{x-l}{r}\right)+1\right]\right\}\times\frac{1}{2}\left\{\left[erf\left(\sqrt{\pi}\,\frac{y}{r}\right)+1\right]\right. \\
&\quad \left.-\left[erf\left(\sqrt{\pi}\,\frac{y-L}{r}\right)+1\right]\right\} \\
&= W_{\max}C_{(x)}C_{(y)},
\end{aligned}
\tag{6}
$$

where $C_{(x)}, C_{(y)}$ refer to the subsidence distribution coefficients of the trend and tendency, respectively.

The working face is a rectangular mining area, the mining length along the strike is $l = 540m$, the mining width along the strike is $L = 136m$, and the main influence radius of the mining is $r = 98m$, The coordinate system is established with the lower left corner of the mining area as the coordinate origin as of the coordinate system (Figure 5): The maximum settlement value of the main section is measured to be $W_0 = 1318mm$.

3.2.1. Prediction Error of the Distribution of the Surface Settlement along the Inclined Observation Lines. According to the observation data, the settlement coefficient is determined as $q = 0.73$, the tangent of the main influence angle is determined as $\tan\beta = 2.2$, and the subsidence at any point on the surface is calculated using (6). Figure 6 shows all the predicted and measured values of the inclination parallel observation lines. It can be found out that the predictions of each observation line in the inclined direction deviate clearly from the actual subsidence curve, with similarity shown only around the maximum subsidence values.

The Root Mean Square Error (RMSE) [31]and the Percent Relative Error (PRE) [32]are adopted to examine how subsidence is accurately and reliably predicted by using the formula for each observation line at any point in the surface. As a numerical measure of prediction accuracy, RMSE refers to the square root of the sum of the squares of the difference between predicted and measured values and the ratio of the number of observations n. A smaller RMSE value indicates a higher accuracy of prediction [33]. The PRE is advantageous in reflecting the reliability of the predicted formula, with a lower absolute value of PRE indicating a greater reliability.

$$
\begin{aligned}
\mathrm{RMSE} &= \pm\sqrt{\frac{\sum[\Delta\Delta]}{n}} \\
\mathrm{PRE} &= \Delta/L' \times 100\%,
\end{aligned}
\tag{7}
$$

where Δ is the true error between predicted and measured values and L' is the measured value.

Table 6 shows the calculation of the RMSE and PRE between the predicted value and the measured value of the surface subsidence along the inclination parallel observation lines. In general, the RMSE of the predicted values of the subsidence for observation lines is high in the inclined direction. However, according to the PRE, the prediction accuracy of the inclined direction observation lines shows a gradual trend of increasing from the center of the subsidence basin to the edge.

3.2.2. Prediction Error of the Distribution of the Surface Subsidence along the Strike Parallel Observation Lines. Figure 7 shows the comparison between the predicted and measured values of all the strike parallel observation lines. It can be discovered that the predictions of observation lines A and B at the center of the subsidence basin are relatively close to the measured subsidence curves, despite a significant difference in the observation line subsidence curves toward the edge of the basin.

Table 7 shows the measured and predicted distribution of the surface subsidence along the strike parallel observation lines as well as the RMSE and PRE. To be specific, RMSE is predicted to be the minimum for the A-line subsidence toward the main section. When shifting away from the center line of the subsidence basin, the RMSE for the other observations increases first and then decreases. However, judging from the PRE, the prediction accuracy of the strike line reaches the highest in the center of the basin and it increases gradually when moving away from the center of the subsidence basin.

According to the comparison in subsidence prediction and RMSE between the actual measurement data and the

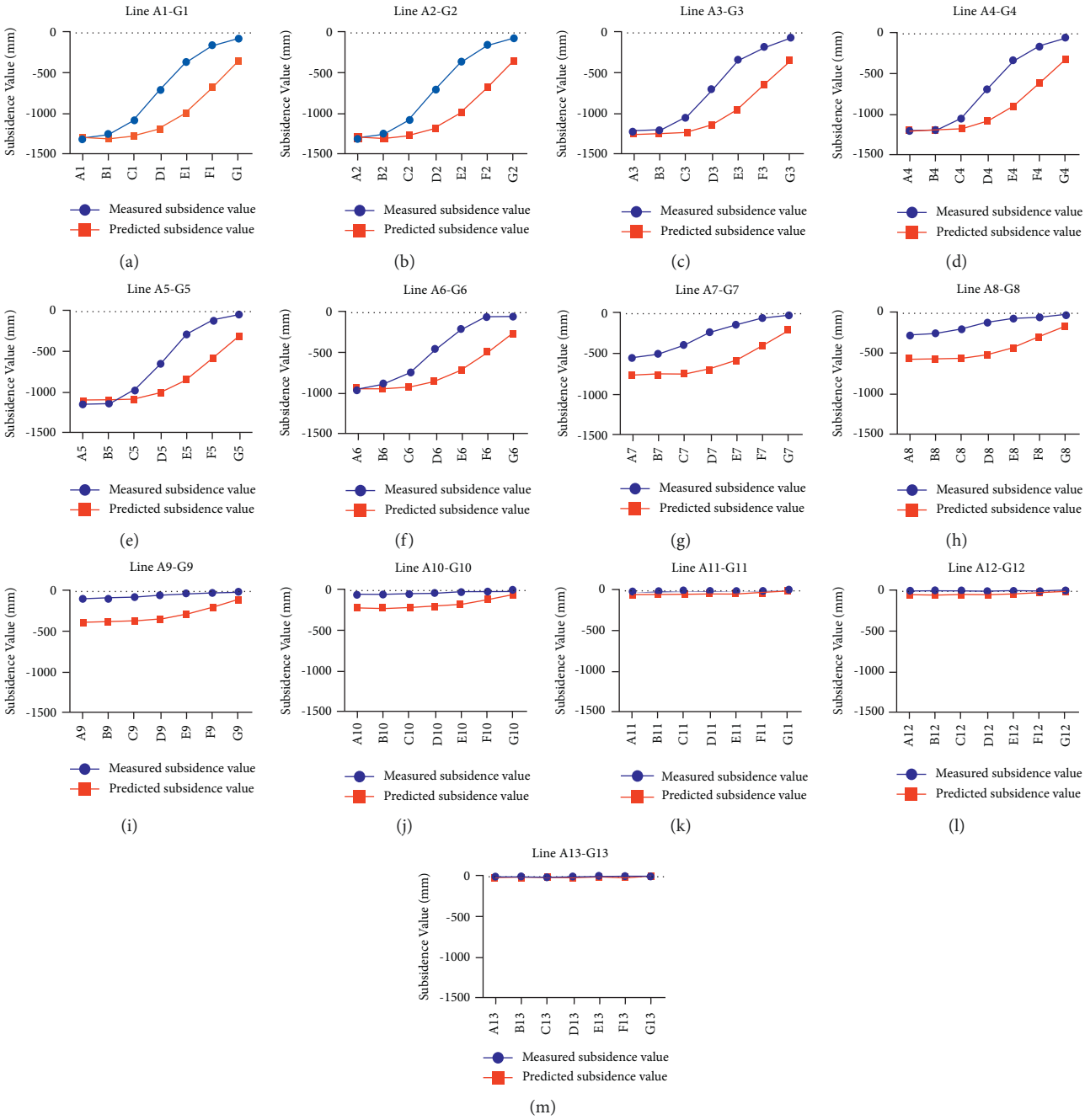

Figure 6: The measured and predicted distribution of the surface subsidence along the inclination parallel lines.

Table 6: Predicted errors of each line in the inclined direction.

Observation lines	Measured mean value/mm	RMSE of predicted/(mm)	PRE%
Line A1–G1	−712.43	380.34	43.26
Line A2–G2	−705.97	380.71	43.94
Line A3–G3	−673.48	363.14	44.00
Line A4–G4	−676.51	333.54	38.74
Line A5–G5	−621.47	320.15	41.74
Line A6–G6	−479.05	314.97	53.71
Line A7–G7	−272.20	335.76	117.67
Line A8–G8	−135.53	315.56	224.74
Line A9–G9	−53.82	254.37	452.33
Line A10–G10	−32.51	149.32	436.30
Line A11–G11	−18.30	28.95	147.53
Line A12–G12	−11.78	40.40	317.56
Line A13–G13	−12.27	8.27	60.00

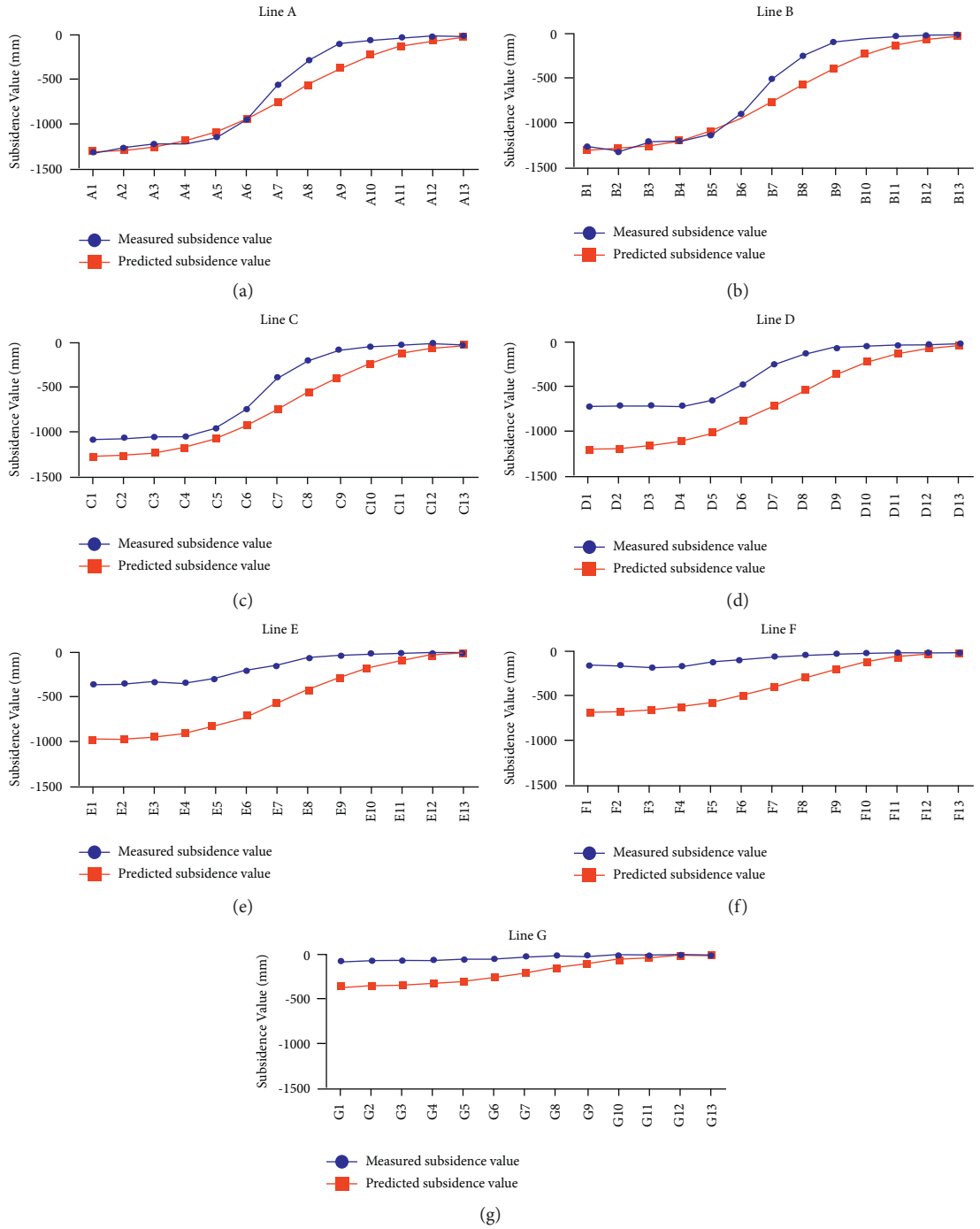

Figure 7: The measured and predicted distribution of the surface subsidence along the strike parallel observation lines.

Table 7: Predicted relative errors of each line in the strike direction.

Observation line	Measured mean value (mm)	RMSE of predicted (mm)	PRE%
Line A	−626.41	139.55	15.37
Line B	−612.71	153.46	17.72
Line C	−517.29	207.28	34.58
Line D	−336.94	354.16	92.78
Line E	−168.95	436.50	219.78
Line F	−81.69	346.23	353.46
Line G	−36.43	192.14	436.92

prediction result for each observation line, it can be known that the subsidence prediction formula at any point on the surface has lower RMSE and higher prediction accuracy in the central part of the subsidence basin. In the region which is more distant from the center of the subsidence basin, however, the RMSE of the predicted values is larger and the level of prediction accuracy is lower.

4. Discussion and Conclusion

4.1. Discussion. At present, most of the research focuses on linear observation stations, analyzing only the law of subsidence for the main section of the subsidence basin. Consequently, there is little research on the law of subsidence in other areas of the subsidence basin. In this study, the historical subsidence monitoring data of the network observation station is reanalyzed. According to the research results, the subsidence in the central area of the subsidence basin conforms to normal distribution law, not that on the edge of the subsidence basin. Such a deviation is related to the exact ground structure. The mining depth of the working face in the study area is 132 m, but the thickness of the Quaternary loose layer in the overlying strata is 71 m, which is relatively large. To some extent, this will contribute to the occurrence of surface subsidence [34–36].

As a highly complex mechanical and spatiotemporal process, the surface subsidence caused by mining is attributed to many factors, which in turn affects the distribution law of subsidence. According to the superposition principle of mining influence, mining surface subsidence can be regarded as the superposition of multiple independent unit mining, with each unit mining having limited impact on the overall subsidence. Therefore, the stratum subsidence caused by underground coal seam mining basically conforms to normal distribution. Therefore, it is universally reasonable to apply the normal distribution function as the mining surface subsidence influence function [37, 38].

Due to the exact geological conditions of mining, which affects how surface subsidence develops, the surface subsidence may not fully conform to normal distribution. Therefore, it is necessary to evaluate the geological mining conditions in the first place when the probability integral method based on the normal distribution is adopted. Under exceptional geological conditions, such as the stratum that contains thick topsoil or thick and hard, it is necessary to modify the model parameters of the probability integral method, or introduce other distribution functions and probability integral method into the construction of a combined model for the improvement of prediction accuracy.

5. Conclusion

In this paper, the field measurement data of the network observation station are analyzed through statistical methods, so as to explore the law of subsidence in the whole subsidence basin. Furthermore, the following conclusions are drawn.

(1) By conducting Kurtosis–Skewness normality test and K–S normality test, the subsidence data of each observation line of network observation are analyzed. On this basis, it is concluded that the surface subsidence caused by coal mining usually conforms to normal distribution, rather than the subsidence of observation line A13-G13 at the edge of subsidence basin. Besides, the subsidence of all other observation lines conforms to normal distribution.

(2) The prediction equation intended for the calculation of surface settlement at any point is used to predict the settlement along the observation lines of the observation station network. According to the calculation results, the relative error is the least significant for the equation used to predict the surface settlement at any point through the probability integral method. In the strike direction, the PRE is 15.37% for the settlement prediction of the observation line a, and the PRE reaches the maximum of 436.92% for the observation line *f*. As the observation line shifts away from the center of the sinking basin, the PRE increases progressively. In the tilt direction, there is a small PRE of the four observation lines A1–G1 to A5–G5 close to the center of the basin, reaching about 40%, which indicates high reliability. Then, as the observation line shifts away from the center of the basin, it gradually increases, with the PRE of the observation line A9–G9 reaching a maximum of 452.33%. Judging from the change of PRE in the comprehensive strike and tilt direction, PRE gradually increases from the center of the basin to the edge of the basin. That is to say, the reliability of probability integral method in predicting the subsidence at any point on the surface diminishes gradually from the center of the basin to the edge of the basin.

(3) When the surface subsidence prediction method is adopted that is based on normal distribution as the mining influence function, it is necessary to take into account the particularity of geological mining conditions and the possibility of prediction deviation. Due to the limited observation data involved, it is necessary to further explore the law of surface subsidence under extraordinary geological mining conditions.

Data Availability

Data will be available on request.

Conflicts of Interest

The authors declare that they have no conflicts of interest.

Acknowledgments

This research was supported by the National Natural Science Foundation of China (Grant no. 41771542) and the National Public Welfare Industry Research Project (Grant No. 200911015–3). All of the financial support provided is gratefully acknowledged.

References

[1] J. Li, S. Chen, Y. Wu et al., "How to make better use of intermittent and variable energy? A review of wind and photovoltaic power consumption in China," *Renewable and Sustainable Energy Reviews*, vol. 137, no. 2020, p. 110626, 2021.

[2] X. Ruhang, S. Zixin, T. Qingfeng, and Y. Zhuangzhuang, "The cost and marketability of renewable energy after power market reform in China: a review," *Journal of Cleaner Production*, vol. 204, pp. 409–424, 2018.

[3] Z. Jia and B. Lin, "How to achieve the first step of the carbon-neutrality 2060 target in China: the coal substitution perspective," *Energy*, vol. 233, p. 121179, 2021.

[4] G. Li, Z. Hu, P. Li, D. Yuan, W. Wang, and K. Yang, "The optimal framework and model to balance underground coal mining and cropland protection in Jining, eastern China," *Resources Policy*, vol. 74, no. April, p. 102307, 2021.

[5] J. Wang, S. S. Peng, and Y. Li, "State-of-the-art in underground coal mining and automation technology in the United States," *Journal of China Coal Society*, vol. 46, no. 1, pp. 36–45, 2021.

[6] G. Li, Z. Hu, P. Li et al., "Innovation for sustainable mining: integrated planning of underground coal mining and mine reclamation," *Journal of Cleaner Production*, vol. 351, no. 2021, p. 131522, 2022.

[7] G. A. H. Die, *Theorie der Bodensenkungen in Kohlengebi - eten mit besonderer Berücksichtigung der Eisenbahnsenkungen des Ostrau-Karwiner Steinkohlenrevieres*, Springer-Verlag, Berlin, 1913.

[8] J. Yue, M. Rafal, P. Li, X. Yuan, S. Anton, and Y. Jiang, "Summary and development of mining subsidence theory," *Mental Mine*, vol. 520, pp. 1–7, 2019.

[9] Y. Jiang, R. Misa, K. Tajduś, A. Sroka, and Y. Jiang, "A new prediction model of surface subsidence with Cauchy distribution in the coal mine of thick topsoil condition," *Archives of Mining Sciences*, vol. 65, no. 1, pp. 147–158, 2020.

[10] L. Yucheng and D. Huayang, "Hyperbolic function model for predicting the main section surface deformation curve due to approximate horizontal coal seam underground longwall mining," *Journal of China University of Mining and Technology*, vol. 48, no. 3, pp. 676–681, 2019.

[11] K. Tajdus, A. Sroka, R. Misa, A. Tajdus, and S. Meyer, "Surface deformations caused by the convergence of large underground gas storage facilities," *Energies*, vol. 14, no. 2, p. 402, 2021.

[12] A. Sroka, S. Knothe, K. Tajduś, and R. Misa, "Point movement trace vs. The range of mining exploitation effects in the rock mass," *Archives of Mining Sciences*, vol. 60, no. 4, pp. 921–929, 2015.

[13] A. Sroka, R. Misa, and K. Tajduś, "Determination of the horizontal deformation factor for mineral and fluidized deposits exploitation," *Acta Geodynamica et Geomaterialia*, vol. 15, no. 1, pp. 23–26, 2017.

[14] J. Litwiniszyn, *Stochastic Methods in Mechanics of Granular Bodies*, Springer, Wien, 1974.

[15] B. Liu and G. Liao, *Basic Law of Surface Movement in Coal Mines*, China Industrial Press, Beijing,China, 1965.

[16] X. Tan, B. Song, H. Bo, Y. Li, M. Wang, and G. Lu, "Extraction of irregularly shaped coal mining area induced ground subsidence prediction based on probability integral method," *Applied Sciences*, vol. 10, no. 18, pp. 6623–6640, 2020.

[17] P. Li, D. Peng, Z. Tan, and K. Deng, "Study of probability integration method parameter inversion by the genetic algorithm," *International Journal of Mining Science and Technology*, vol. 27, no. 6, pp. 1073–1079, 2017.

[18] G. Wang, P. Li, Q. Wu, X. Cui, and Z. Tan, "Numerical simulation of mining-induced damage in adjacent tunnels based on FLAC3D," *Advances in Civil Engineering*, vol. 2021, pp. 1–21, 2021.

[19] P. Li, L. Yan, and D. Yao, "Study of tunnel damage caused by underground mining deformation: calculation, analysis, and reinforcement," *Advances in Civil Engineering*, vol. 2019, pp. 1–18, 2019.

[20] H. Li, B. Zhao, G. Guo, J. Zha, and J. Bi, "The influence of an abandoned goaf on surface subsidence in an adjacent working coal face: a prediction method," *Bulletin of Engineering Geology and the Environment*, vol. 77, no. 1, pp. 305–315, 2018.

[21] Y. Fu, J. Shang, Z. Hu et al., "Ground fracture development and surface fracture evolution in n00 method shallowly buried thick coal seam mining in an arid windy and sandy area: a case study of the ningtiaota mine (China)," *Energies*, vol. 14, pp. 7712–22, 2021.

[22] Y. Yuan, H. Li, H. Zhang, Y. Zhang, and X. Zhang, "Improving reliability of prediction results of mine surface subsidence of northern pei county for reusing land resources," *Applied Sciences*, vol. 10, no. 23, pp. 8385–8397, 2020.

[23] P. Li, W. Zhu, and Z. Xie, "Diverse and divergent influences of phenology on herbaceous aboveground biomass across the Tibetan Plateau alpine grasslands," *Ecological Indicators*, vol. 121, p. 107036, 2021.

[24] G. Li, "Optimal layout of underground coal mining with ground development or protection: a case study of Jining, China," *Resources Policy*, March, vol. 76, , p. 102639, 2022.

[25] K. Deng, Z. Tan, Y. Jiang, H. Dai, Y. Shi, and L. Xu, *Deformation Monitoring and Subsidence Engineering*, China University of Mining and Technology Press, Xuzhou,China, 2014.

[26] W. Zhang, D. Zhang, D. Qi, Z. He, and X. Duan, "A mechanical analysis of support instability risk along the strike of coalface in thick coal seam with large dip angle: a case study," *Earth Sciences Research Journal*, vol. 25, no. 1, pp. 101–108, 2021.

[27] W. Zhang, J. Guo, K. Xie et al., "Comprehensive technical support for safe mining in ultra-close coal seams: a case study," *Energy Exploration & Exploitation*, vol. 39, no. 4, pp. 1195–1214, 2021.

[28] W. Yang and T. Zhang, *Introduction and Application of SPSS Statistical Analysis*, Tsinghua University Press, Beijing,China, 2022.

[29] W. Jijun, R. Guoyu, K. Xiaoyan, and W. Fang, "Normality analysis of the monthly and annual precipitation in henan province," *Climatic and Environmental Research (in Chinese)*, vol. 15, no. 4, pp. 522–528, 2010.

[30] S. R. Naganna and P. C. Deka, "Variability of streambed hydraulic conductivity in an intermittent stream reach regulated by Vented Dams: a case study," *Journal of Hydrology*, March, vol. 562, , pp. 477–491, 2018.

[31] T. Chai and R. R. Draxler, "Root mean square error (RMSE) or mean absolute error (MAE)? -Arguments against avoiding RMSE in the literature," *Geoscientific Model Development*, vol. 7, no. 3, pp. 1247–1250, 2014.

[32] M. Wiberg, W. J. Van Der Linden, and A. A. Von Davier, "Local observed-score kernel equating," *Journal of Educational Measurement*, vol. 51, no. 1, pp. 57–74, 2014.

[33] D. S. K. Karunasingha, "Root mean square error or mean absolute error? Use their ratio as well," *Information Sciences*, vol. 585, pp. 609–629, 2022.

[34] Z. Dawei, W. Kan, B. Zhihui et al., "Formation and development mechanism of ground crack caused by coal mining: effects of overlying key strata," *Bulletin of Engineering Geology and the Environment*, vol. 78, no. 2, pp. 1025–1044, 2019.

[35] D. Zhou, K. Wu, X. Miao, and L. Li, "Combined prediction model for mining subsidence in coal mining areas covered with thick alluvial soil layer," *Bulletin of Engineering Geology and the Environment*, vol. 77, no. 1, pp. 283–304, 2018.

[36] J. Ma, D. Yin, N. Jiang, S. Wang, and D. Yao, "Application of a superposition model to evaluate surface asymmetric settlement in a mining area with thick bedrock and thin loose layer," *Journal of Cleaner Production*, vol. 314, no. June, p. 128075, 2021.

[37] S. Ju, S. Shiqian, and P. Chenyi, *Probability Theory and Mathematical Statistics*, Higher Education Press, Beijing, 4th Edition, 2008.

[38] C. Xiru, *Probability Theory and Mathematical Statistics*, China University of science and Technology Press, Hefei, 2009.